Supporting Information

Choi et al. 10.1073/pnas.1018790108

SI Materials and Methods

Histology. Mice were killed under deep anesthesia by transcardial perfusion with PBS, followed by fixation with 4% formalin in phosphate buffer. Brains were removed, immersed in 4% formalin in phosphate buffer overnight, and then transferred to a 30% sucrose solution for at least 3 d. Target regions were navigated by stereotaxic coordinates and fluorescence, followed by sectioning into 30-μm coronal sections on a freezing sliding microtome. The sections were stained using the Nissl method or immunostaining and mounted on glass slides for microscopic evaluation.

Dorsal Skinfold Chamber Model. A small dorsal skinfold chamber kit (SM100) was purchased from APJ Trading, and surgery was performed as described previously (1). In brief, mice were anesthetized with an i.p. injection of ketamine–xylazine, the dorsal skin was extended, and two mirror-image titanium frames were mounted. One layer of skin was excised, leaving the striated muscle of the opposite side intact, and then replaced with a glass coverslip mounted into the frame.

1. Isaka N, Padera TP, Hagendoorn J, Fukumura D, Jain RK (2004) Peritumor lymphatics induced by vascular endothelial growth factor-C exhibit abnormal function. *Cancer Res* 64:4400–4404.

In Vivo Skull Imaging Preparation. After anesthesia with an i.p. injection of ketamine-xylazine, the scalp was removed, and the mouse head was fixed to a stereotaxic frame.

In Vivo Ear Imaging Preparation. After anesthesia with an i.p. injection of ketamine-xylazine, the ear was glued to a glass and placed on a custom-designed mount.

Intravenous Administration. All dyes were injected i.v. through the lateral tail vein or the retro-orbital venous sinus. An i.v. catheter was used when timely injection was necessary. For the plasma marker, 100 μL of 2% wt/wt dextran-conjugated dye was administered as indicated. To determine the dose of dye for i.v. injection, we multiplied the dilution factor for plasma by the conventional dose of the dye used for tissue staining and modified it experimentally. The following dyes were used: OGB-1:00 AM (Invitrogen; 50 μL of 100 μg), Hoechst (20 mg/kg), SR101 (Invitrogen; 10 μL of 0.5 mg/mL), adenovirus (100 μL of 1×10^9 pfu of adenoviral vector with CMV promoter-driven GFP expression), Quantum Dot (Q21021MP, Molecular Probes; 20 μL of 2 μM), TAMRA-MION (50 μL of 10 μM), and siRNA (60 μL of 125 pmol mixed with 60 μL of 2% in vivo jetPEI; Polyplus).

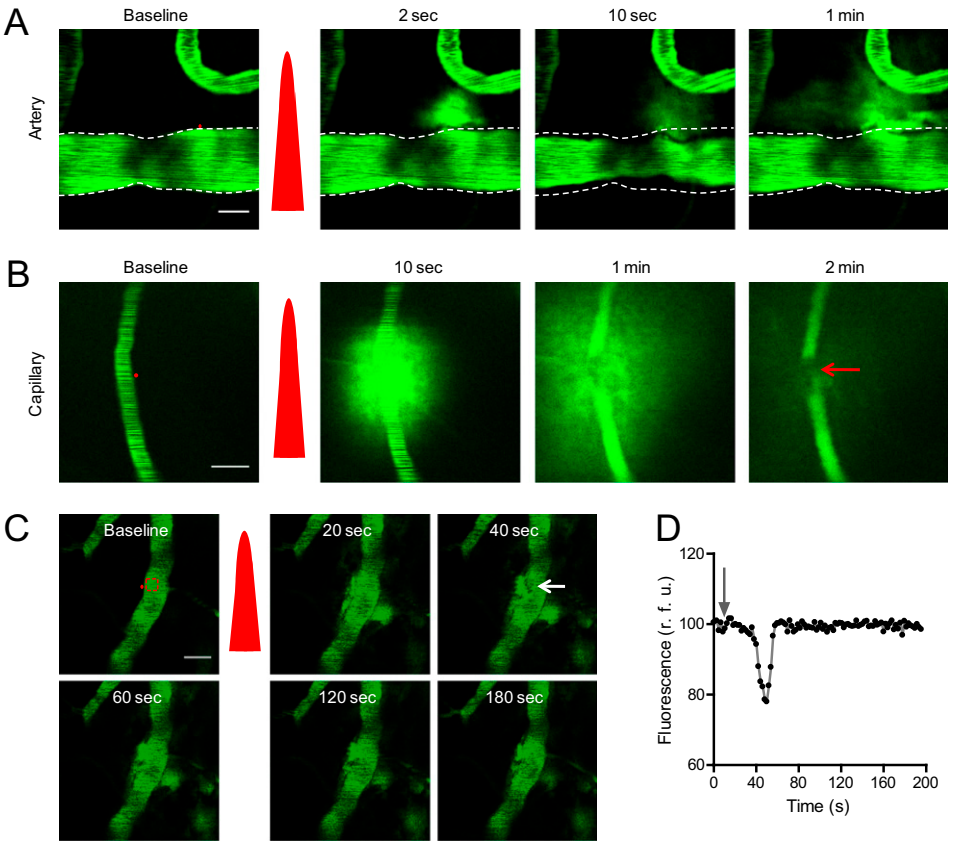

Fig. S1. (*A*) Laser-induced extravasation in an artery. Arterial stimulation accompanied arterial contraction. The dashed line demarcates the baseline lumen area. (Scale bar: 50 μm.) (*B*) Laser-induced extravasation in a capillary. Capillaries were vulnerable to hemorrhage when irradiated. Note the loss of dark streaks, indicating red blood cell movement; a clot formed around the irradiated region (red arrow). (Scale bar: 10 μm.) (*C*) Transient clot formation after laser irradiation. During laser-induced vascular permeabilization, transient clot formation (white arrow) was observed with disturbed downstream blood flow. The red dot indicates the position of laser irradiation. (Scale bar: 20 μm.) (*D*) Temporal dynamics of fluorescence intensity in the boxed region shown in *C*. The arrow indicates the time of laser irradiation.

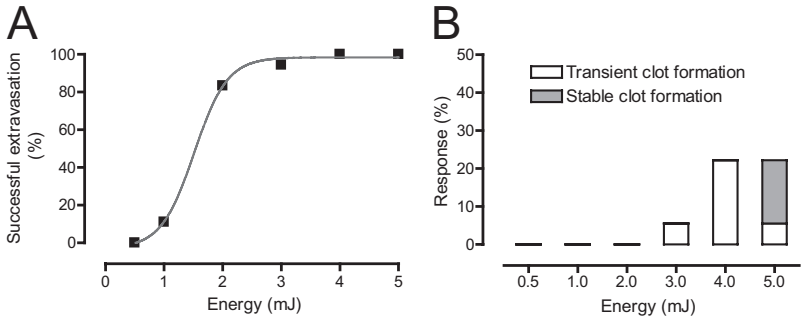

Fig. S2. (*A*) Relationship between laser energy and the probability of successful extravasation (n = 18 for each dose of laser energy in three mice). (*B*) Dependence of clot formation on laser energy (n = 18 for each dose of laser energy in three mice).

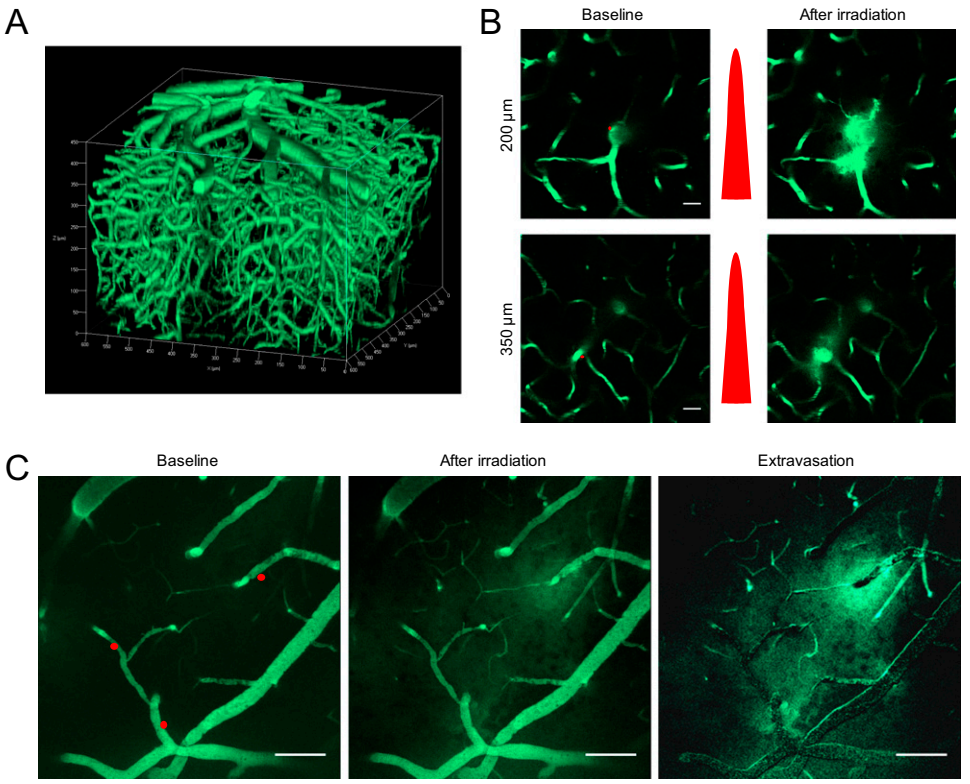

Fig. S3. Feasibility of laser-induced extravasation in the deep cortical layer and to a large area. (*A*) 3D view of vascular structure in the cortex. The skull and dura layer were removed, 2 MDa of FITC-dextran was i.v. injected, and images were obtained at 3-μm intervals to a depth of 450 μm. (*B*) Laser-induced extravasation in the deep cortical layers. (Scale bar: 20 μm.) (*C*) Molecular delivery to a large area by irradiation of multiple blood vessels. Here 70 kDa of FITC-dextran was injected i.v. in the thinned-skull window model, and three extravasations were induced by irradiating three regions in the pial venules. (Scale bar: 100 μm.)

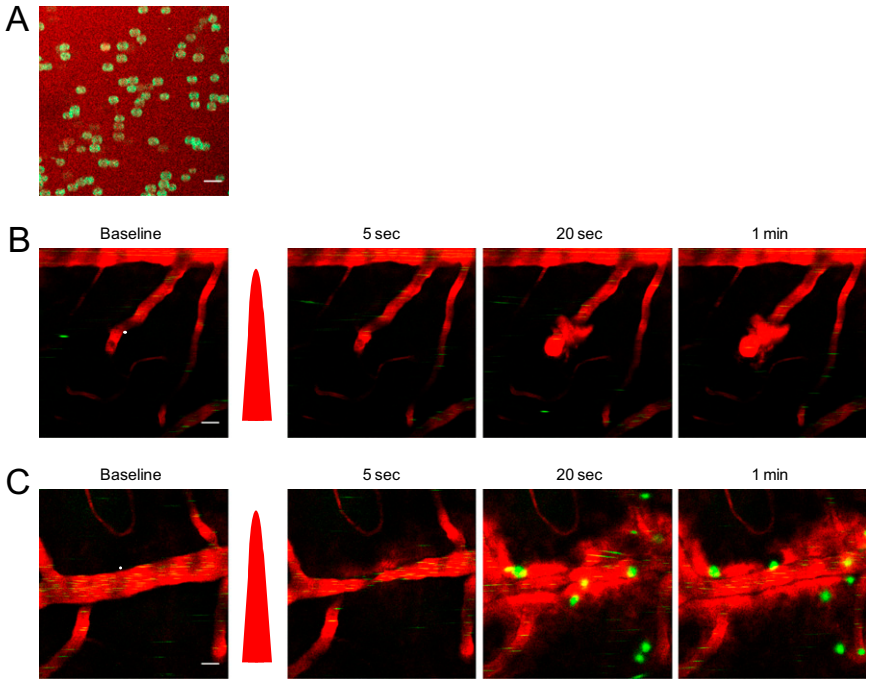

Fig. S4. Red blood cells (RBCs) did not leak during laser-induced vascular permeabilization. RBCs were stained and injected i.v. with TRITC-dextran. (*A*) Stained RBCs (green) in TRITC-dextran (red) solution. (Scale bar: 10 μm.) (*B*) RBCs did not leak during laser-induced vascular permeabilization. Green streaks represent movement of stained RBCs. (Scale bar: 20 μm.) (*C*) RBC leakage during severe arterial contraction by laser irradiation. Severe contraction was induced by RBC leakage after laser irradiation to the artery, as denoted by the clear circular green signals outside of the lumen. (Scale bar: 20 μm.)

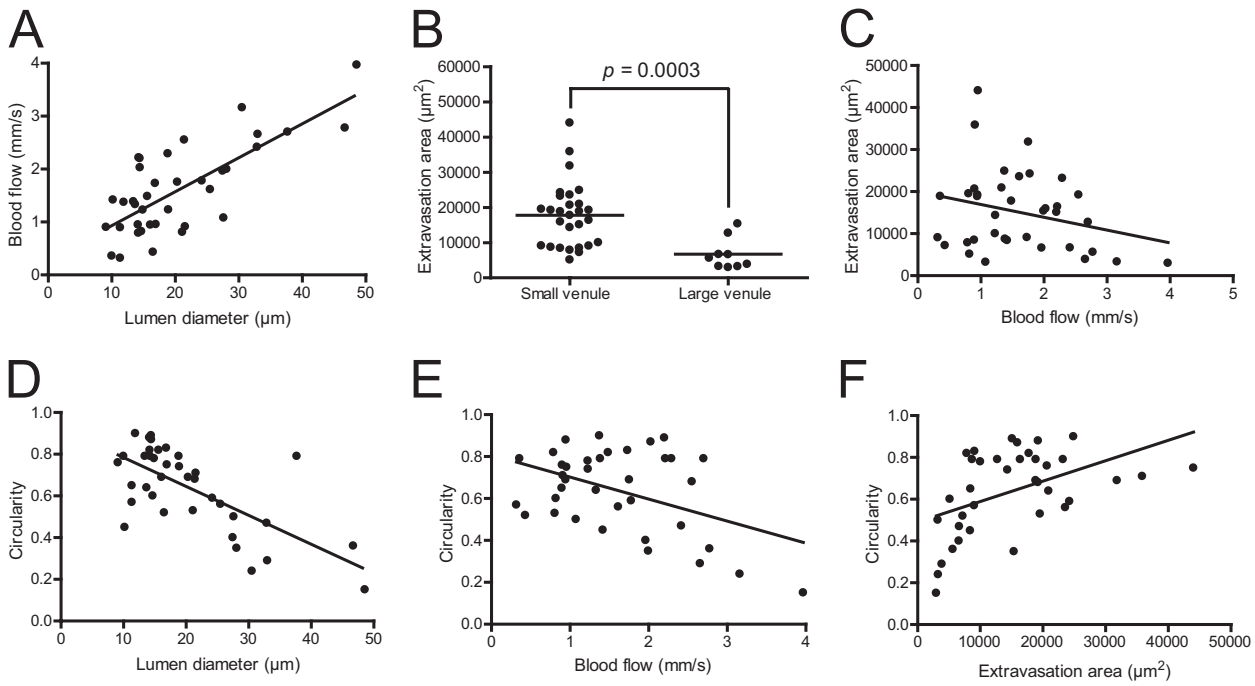

Fig. S5. Characterization of laser-induced extravasation. Lumen diameter and blood flow were measured at baseline, and the extravasation area and circularity of the extravasation area were quantified based on an image obtained at 1 min. (*A*) Lumen diameter and blood flow in venules showed a strong positive correlation ($R^2 = 0.5612$; $P < 0.0001$; $n = 37$). (*B*) Compared with large venules (lumen diameter <25 μm; $n = 28$), small venules (lumen diameter >25 μm; $n = 9$) showed significantly less extravasation area ($P = 0.0003$). (*C*) Blood flow had a nonsignificant negative correlation with extravasation area ($R^2 = 0.0718$; $P = 0.1089$) (*D* and *E*) Smaller venules or venules with slower blood flow had more circular extravasation ($R^2 = 0.4721$; $P < 0.0001$ vs. $R^2 = 0.1988$; $P = 0.0057$). (*F*) The extravasation area was positively correlated with the circularity of extravasation ($R^2 = 0.2232$; $P = 0.0032$).

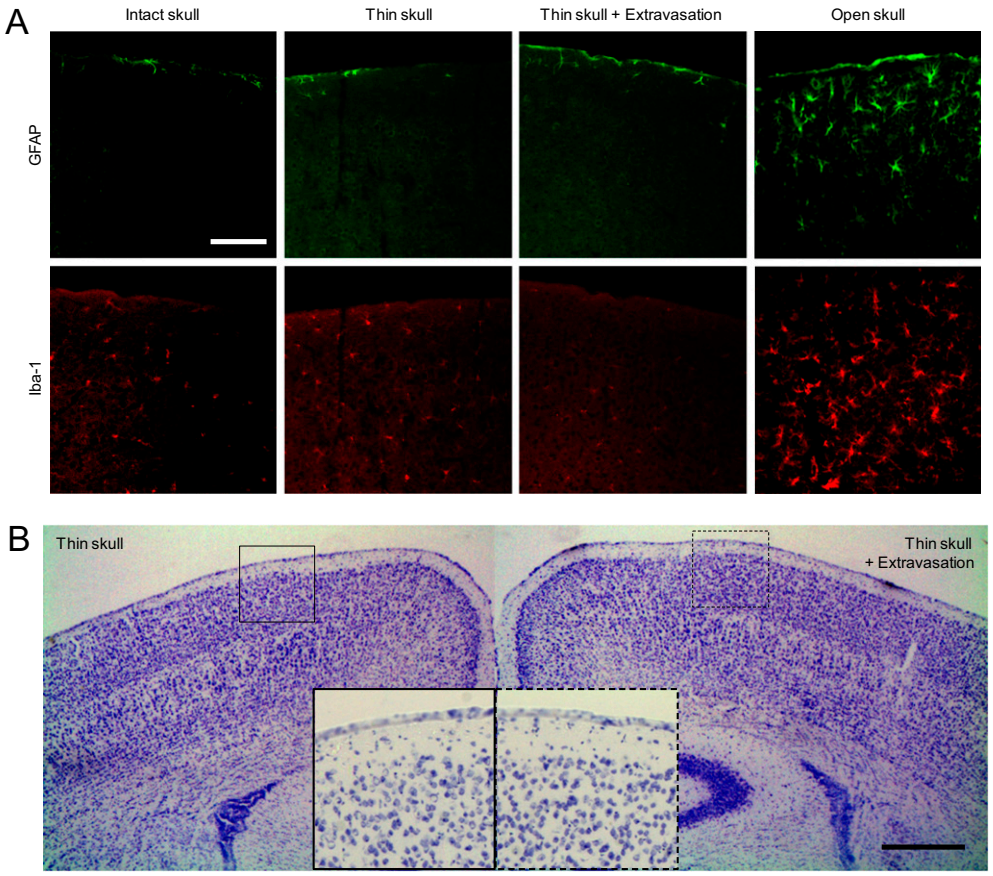

Fig. S6. Assessment of delayed cell death and immune response at 2 d after laser-induced extravasation. (*A*) Nissl staining. Thinned-skull windows (~1 mm in diameter) were made in each hemisphere, and extravasation was induced in the right hemisphere. (*Insets*) Magnified views of the thinned-skull windows regions. (Scale bar: 500 μm.) (*B*) Immunostaining of astrocyte (GFAP) and microglial (Iba-1) activation. (Scale bar: 100 μm.)

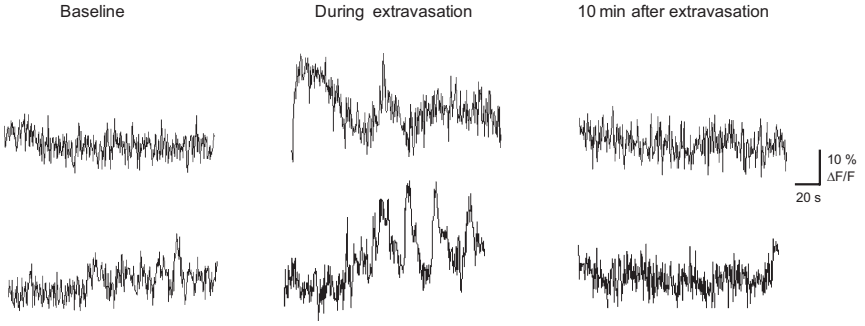

Fig. S7. Functional calcium activity of astrocytes during laser-induced plasma leakage. A calcium indicator (OGB-1:00 AM) and astrocyte marker (SR101) were loaded in the cortex using a conventional bath-loading method. Rhodamine was administered i.v. as a plasma indicator. Astrocyte calcium activity was measured with a 2-Hz acquisition rate. Spontaneous calcium activity in astrocytes is shown.

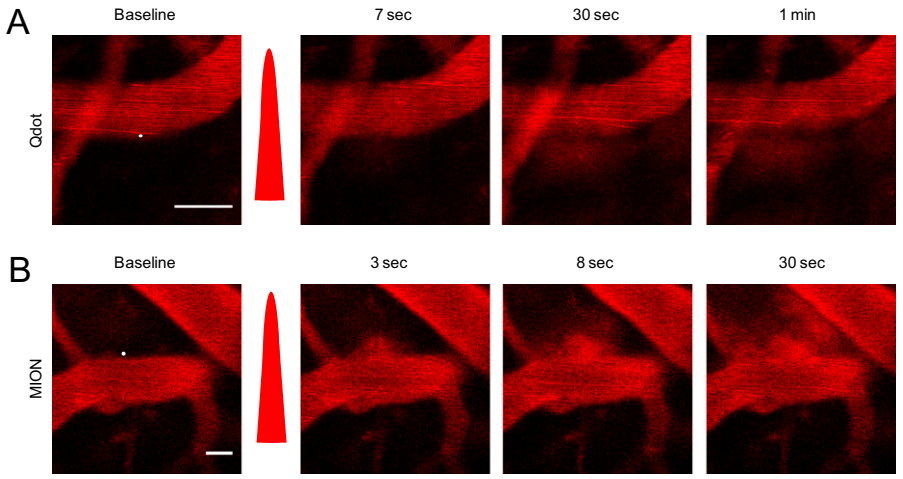

Fig. S8. Laser-induced permeabilization of nanoparticles. (*A*) Quantum dot. (*B*) TAMRA- conjugated MiONs.

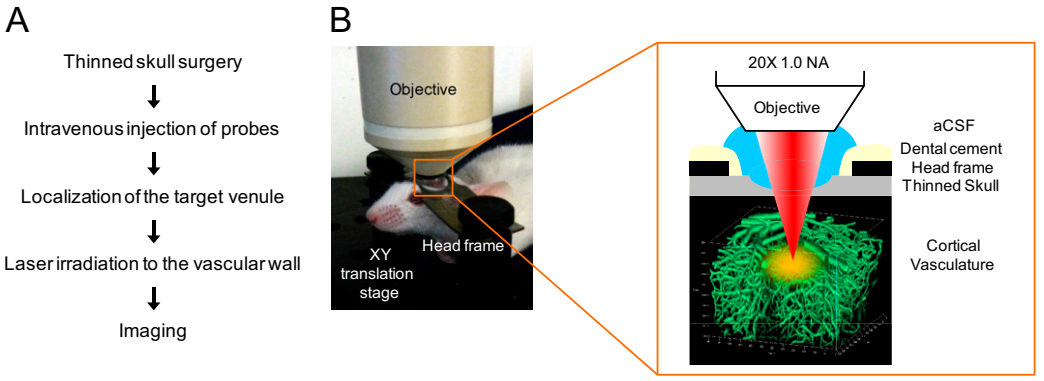

Fig. S9. Experimental setup. (*A*) Procedure for the laser-induced extravasation experiments. (*B*) Schematic diagram of the experimental setup.